NANO LETTERS

2007
Vol. 7, No. 2
363−366

Current-Driven Phase Oscillation and Domain-Wall Propagation in $W_xV_{1-x}O_2$ Nanobeams

Qian Gu,[†,‡] Abram Falk,[†,§] Junqiao Wu,[‡] Lian Ouyang,[‡] and Hongkun Park*[,‡,§]

Department of Chemistry and Chemical Biology and Department of Physics, Harvard University, 12 Oxford Street, Cambridge, Massachusetts 02138

Received October 22, 2006; Revised Manuscript Received January 12, 2007

ABSTRACT

We report the observation of a current-driven metal (M)–insulator (I) phase oscillation in two-terminal devices incorporating individual $W_xV_{1-x}O_2$ nanobeams connected to parallel shunt capacitors. The frequency of the phase oscillation reaches above 5 MHz for ~1 μm long devices. The M–I phase oscillation, which coincides with the charging/discharging of the capacitor, occurs through the axial drift of a single M–I domain wall driven by Joule heating and the Peltier effect.

First-order solid−solid phase transitions underlie many technologically important material properties, such as ferroelectricity and the metal−insulator transition (MIT). The phase transitions in bulk and thin-film materials occur through heterogeneous domain nucleation and expansion, and materials undergoing repeated phase transitions thus develop complicated domain boundaries and often become polycrystalline.[1−4] Despite its critical importance in determining the functional characteristics of a material, the dynamics at the domain boundary has been difficult to investigate because domain nucleation and organization cannot be controlled in bulk systems.

In contrast, nanoscale materials with one or more dimensions smaller than a typical domain size do not support multiple domains along the confined directions and exhibit phase transition behaviors that differ significantly from their bulk counterparts.[2−7] These materials therefore provide excellent model systems for examining the microscopic mechanism of solid−solid phase transitions as well as the dynamics of individual domains.[2−5]

Here we report the observation of current-driven metal (M)−insulator (I) phase oscillations in two terminal devices incorporating individual $W_xV_{1-x}O_2$ nanobeams connected to parallel shunt capacitors. The frequency (f) of the phase oscillation increases linearly with current and is inversely proportional to the nanobeam length and the capacitance (C) in the circuit. The maximum f of the phase oscillator exceeds 5 MHz for 1 μm long devices when $C \sim 100$ pF. The experimental data suggest that the phase oscillation, which coincides with the capacitor charging/discharging, is dictated by the Joule-heating-induced MIT, heat dissipation, and the Peltier effect, and that the phase oscillation occurs through the axial drift of a single M−I domain wall.[8,9] These observations demonstrate that nanobeams and nanowires can act as essentially one-dimensional systems for domain propagation and provide detailed insight into the microscopic mechanism of domain motion. They also demonstrate that the nanoscale MIT might be used to define the electrical oscillator function in nano- and macroelectronic circuits.

Bulk VO_2 undergoes a Mott MIT at $T_{MIT} \sim 68$ °C.[10−12] Accompanying the MIT is a structural transition of the crystal lattice from a low-temperature (insulating) monoclinic phase to a high-temperature (metallic) tetragonal phase.[10,11] When vanadium is substituted by other transition metal elements, T_{MIT} can be lowered continuously to room temperature and below.[13−15] Pure and doped VO_2 have been suggested as candidates for realizing Mott field-effect transistors[16,17] and thermochromic devices.[13,18]

The single-crystalline $W_xV_{1-x}O_2$ nanobeams employed in this study were synthesized using a variant of the vapor transport method reported previously.[19] Analyses of electron microscopy and X-ray diffraction data, such as those in parts a and b of Figure 1, show that the $W_xV_{1-x}O_2$ nanobeams are single crystalline and that the W atoms are homogenously distributed throughout the nanobeam. The MIT in individual $W_xV_{1-x}O_2$ nanobeams was studied by incorporating them into two- and four-probe geometries using electron-beam lithography (Figure 2a, inset).[20] Figure 1c shows the temperature dependence of the four-probe resistance measured from five nanobeams with increasing W doping levels: T_{MIT} decreases

* To whom correspondence should be addressed. E-mail: Hongkun_Park@harvard.edu.
† These authors contributed equally to this work.
‡ Department of Chemistry and Chemical Biology.
§ Department of Physics.

10.1021/nl0624768 CCC: $37.00
Published on Web 01/26/2007

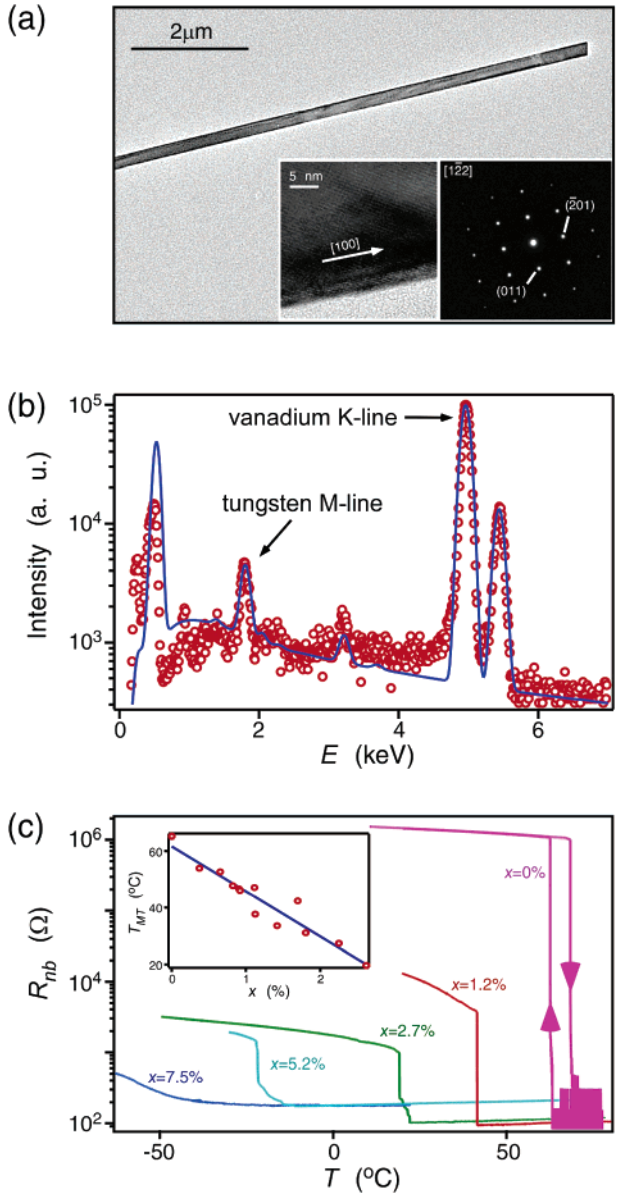

Figure 1. (a) Transmission electron microscopy (TEM) image of a representative $W_xV_{1-x}O_2$ nanobeam. Insets: high-resolution TEM image (left) and selected area electron diffraction (SAED) pattern (right) obtained from the same nanobeam. The SAED pattern, which is indexed to a monoclinic lattice with a zone axis of [1$\bar{2}$2], does not change along the nanobeam length, indicating that the whole nanobeam is a single crystal. (b) Energy dispersive X-ray (EDX) spectrum of a $W_{0.02}V_{0.98}O_2$ nanobeam. The EDX spectrum was simulated at various x values using Desktop Spectrum Analyzer with NIST Standard Reference Database and compared with experimental data. The circles are the experimental EDX data, and the solid line is the simulated EDX spectrum with $x = 0.02$. The EDX spectrum does not change at different spots along the nanobeam, indicating a uniform W doping. (c) The four-probe resistance of five nanobeams. The resistance was measured during cooling, except for the $x = 0$ characteristic, in which both heating and cooling traces are presented to show the hysteresis. Inset: Plot of T_{MIT} vs x. T_{MIT} was measured by averaging the heating and cooling transition temperatures. x was determined by EDX.

at a rate of −18.4 °C/% as x increases, consistent with earlier studies on bulk $W_xV_{1-x}O_2$.[13−15]

Our previous study has shown that VO_2 and $W_xV_{1-x}O_2$ nanobeams do not support multiple M−I domains along their

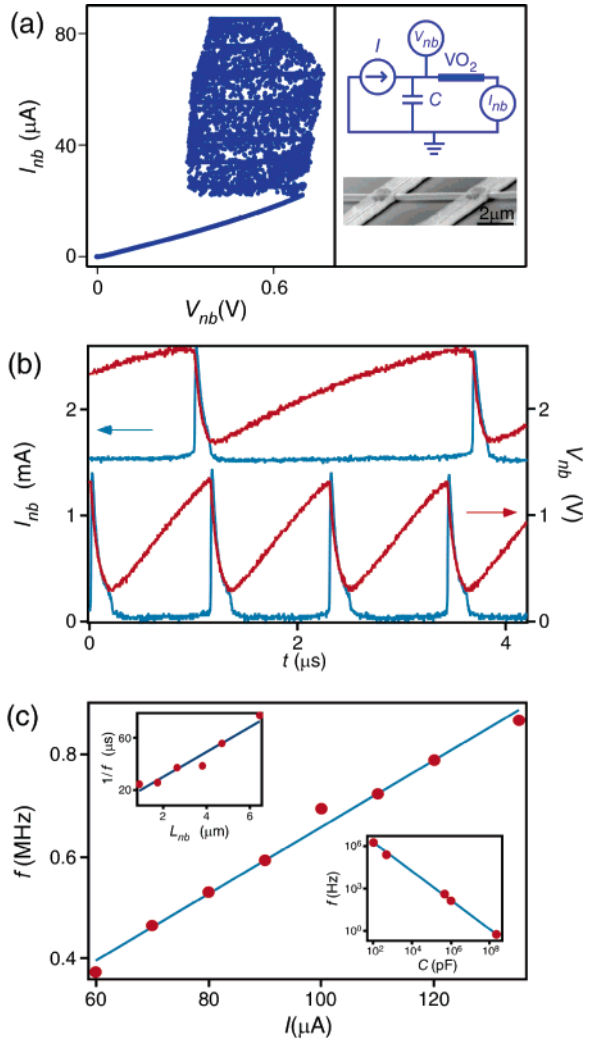

Figure 2. (a) Current (I_{nb})−voltage (V_{nb}) characteristics of a representative, suspended $W_{0.01}V_{0.99}O_2$ nanobeam device under constant I biasing condition. The height (width) of this nanobeam is 100 nm. Upper inset: circuit diagram for constant I biasing. Lower inset: scanning electron microscopy image of a representative suspended nanobeam device. (b) I_{nb} (blue) and V_{nb} (red) oscillations measured from a nanobeam device at two different driving currents. The nanobeam dimensions are 200 nm × 140 nm × 760 nm. (c) Oscillation frequency (f) of the electrical oscillation plotted as a function of I_{nb}, with fixed $C \sim 150$ pF. Upper inset: $1/f$ plotted as a function of the nanobeam length (L_{nb}) with $I = 28$ μA and $C \sim 1$ nF. Lower inset: f as a function of C, with fixed $I = 90$ μA. The solid lines are linear fits to the data.

widths and thus serve as one-dimensional systems for domain organization.[20] The character of the MIT depends drastically on a nanobeam's strain environment. When a nanobeam in contact with a substrate undergoes an MIT, substrate-induced strain causes the spontaneous formation of alternating M−I domains.[20] In contrast, a suspended nanobeam undergoes the temperature-induced MIT as a single domain,[20] as evidenced by a temperature-induced transition that is much sharper than those observed in bulk crystals and on-substrate nanobeams (Figure 1c). All the data presented in this study were obtained from suspended nanobeam devices in vacuum in order to minimize the complications arising from the strain-induced domains.

Figure 2a shows the room-temperature current (I)−voltage (V) characteristics of a representative two-probe $W_{0.01}V_{0.99}O_2$ nanobeam device connected in parallel to a shunt capacitor (the inset to Figure 2a shows a diagram of the driving circuit). In this circuit, C can arise from the measurement apparatus, such as the BNC cables and the voltmeter, or from an externally introduced shunt capacitor. Because of the charging and discharging of C, the current flowing through the nanobeam (I_{nb}) differs from total current I (see Supporting Information). At low I, the device exhibits a behavior consistent with the nanobeam in the I phase. As I is increased above a threshold I_{th} (for a typical 1 μm long nanobeam device, $I_{th} \sim 50$ μA), however, the voltage drop across the device (V_{nb}) develops a rapid, spontaneous oscillation. When I is increased even further, typically two or three times I_{th}, V_{nb} becomes stable again, with the device resistance reaching that of the M phase. The power dissipation of the device at the onset of the V_{nb} oscillation decreases linearly with the ambient temperature T, extrapolating to 0 at $T \sim 50$ °C (T_{MIT} of the $W_{0.01}V_{0.99}O_2$ nanobeam under study) (see Supporting Information).

Figure 2b shows I_{nb} and V_{nb} plotted against time (t) measured from a $W_{0.01}V_{0.99}O_2$ nanobeam device. The V_{nb} waveform has a sawtooth shape, with peaks in I_{nb} coinciding with the rapidly falling portions of the V_{nb} trace. As shown in Figure 2c, f of the V_{nb} (I_{nb}) oscillation is directly proportional to I and is inversely proportional to C and the nanobeam length (L_{nb}). Measurements on multiple devices show that these I, C, and L_{nb} scaling behaviors are common to all suspended devices. The typical f observed from 1−3 μm long nanobeam devices is ~1 MHz when $I \sim 100$ μA and $C \sim 100$ pF.

Whereas the apparent shapes of I_{nb} and V_{nb} waveforms do not depend sensitively on C (and thus f), the time traces of nanobeam resistance ($R_{nb} = V_{nb}/I_{nb}$) plotted in parts a and b of Figure 3 show that the R_{nb} waveform shapes change dramatically with C and f. At high f ($f >$ 500 kHz), R_{nb} oscillates between the values consistent with the nanobeam in the M (low R_{nb}) and I (high R_{nb}) phases with a sawtooth waveform. When f is small (<1 kHz), on the other hand, R_{nb} jumps to a large value at the end of a I_{nb} spike and decreases gradually with time when I_{nb} is small. At intermediate f values, the R_{nb} waveform shapes evolve smoothly between these limiting shapes.

When C exceeds 10 μF, f of a typical nanobeam device is small enough to allow real-time optical interrogations.[20] Video 1, included in Supporting Information, shows that the R_{nb} oscillations in Figure 3b are caused by the conversion and expansion of the I and M phases within a nanobeam, as schematically illustrated in Figure 3. Moreover, the same video shows that the direction of the domain motion depends on the direction of I.

The phase oscillations seen in Figures 2 and 3 are reminiscent of those observed in bulk organic[21] and inorganic materials,[8,22−24] including bulk VO_2.[8,23] The behavior of suspended $W_xV_{1-x}O_2$ nanobeam devices is distinct from these bulk oscillations in several important aspects, however. First, the nanobeam device exhibits a stable phase oscillation with

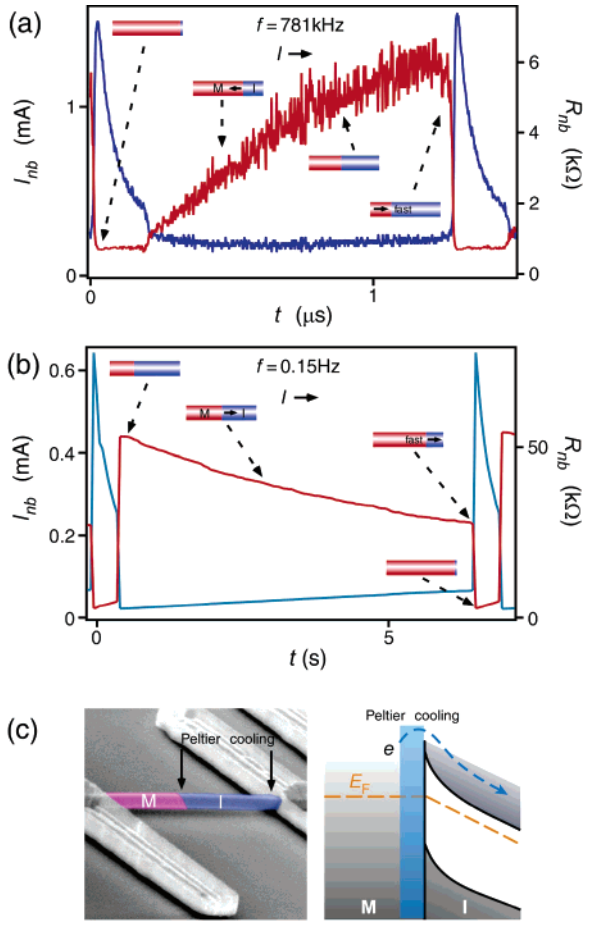

Figure 3. (a) I_{nb} (blue) and R_{nb} (red) traces of the nanobeam from Figure 2 over one cycle. $C = 100$ pF. (b) I_{nb} (blue) and R_{nb} (red) traces of another nanobeam. $C = 220$ μF. The R_{nb} trace is calculated by taking $R_{nb}(t) = V_{nb}(t)/I_{nb}(t)$. (c) Left panel: cartoon showing the domain-wall propagation along the I direction. Right panel: the band diagram at a reverse-biased I−M junction illustrating the Peltier effect. The I phase is drawn as n-type.

f up to 5 MHz. In contrast, the oscillations observed in bulk VO_2 had several different waveform shapes that were unstable, and their f was limited to <5 kHz.[8,23] More importantly, the frequency of the phase oscillations from nanobeam devices obeys well-defined scaling relations with C, I, and L_{nb}: these scaling behaviors have not been observed in previous bulk studies[8,21−24] and provide important experimental clues for the microscopic mechanism underlying the phase oscillation.

Specifically, the data presented in Figures 2 and 3 show that the interplay between the Joule-heating-induced MIT, the capacitor charging/discharging, and heat dissipation is responsible for the V_{nb} and I_{nb} oscillations in $W_xV_{1-x}O_2$ nanobeam devices. When the capacitor is charging, part of I flows through the capacitor instead of the nanobeam. As the charging progresses, however, more I flows through the nanobeam, resulting in a higher Joule heating power. When the temperature reaches T_{MIT}, the nanobeam converts into the M phase. This I-to-M conversion process is self-reinforcing: the metallic nanobeam provides a low-resistance pathway between the capacitor and the ground, causing the capacitor to discharge through the nanobeam (indicated by

the I_{nb} spikes in Figure 2b). As I_{nb} decreases during the capacitor discharge, part of the nanobeam cools and converts back to the I phase, and the cycle restarts.

This phase-oscillation scenario explains the f scaling with I, $1/C$, and $1/L_{nb}$ as well. Figure 2b shows that the rise time (τ_r) of the V_{nb} waveform is generally longer than the fall time (τ_f): this disparity originates because the capacitor charging and discharging rates are determined by $R_{nb}C$ and, while discharging, the nanobeam is in the less-resistive M phase. The observed f variation with I and $1/C$ is a direct reflection of the charging/discharging rate change. Finally, f is proportional to $1/L_{nb}$ because R_{nb} increases linearly with L_{nb}.

The dependence of the shape of the R_{nb} traces on C shown in parts a and b of Figure 3 can be explained, on the other hand, by the difference in the capacitor discharging time relative to the heat dissipation time. When f is high, the discharging is rapid enough that the nanobeam is still cooling after the capacitor has fully discharged and starts recharging. This process leads to an I phase expansion during the charging step. When f is low, part of the nanobeam cools into the I phase before the capacitor has fully discharged. This M-to-I conversion raises R_{nb} and prematurely halts the capacitor discharge. Consequently, at the start of charging, I_{nb} is already large enough to heat the nanobeam and make the M phase grow.

The observation that the direction of the domain motion depends on the direction of I in the optical interrogations (see Supporting Information) indicates that the Peltier effect[8,25] also plays a role in the heat conduction and domain motion processes. As illustrated in Figure 3c, the M−I domain boundary within $W_xV_{1-x}O_2$ and at the Cr−$W_xV_{1-x}O_2$ interface form n-type Schottky barriers.[25,26] Hot electrons crossing the Schottky barrier from the metal (Cr or $W_xV_{1-x}O_2$ M phase) to the $W_xV_{1-x}O_2$ I phase are driven away from the domain boundary by the electric field within the $W_xV_{1-x}O_2$ I phase. These hot electrons therefore carry heat with them, cooling the metal−insulator interface. In devices fabricated from nanobeams resting on the substrate, which have multiple M−I domains,[20] the domains propagate in the direction of I (see video 2 in Supporting Information). A similar effect has been observed in bulk samples and attributed to the M−I Peltier junctions within the $W_xV_{1-x}O_2$ nanobeam locally heating and cooling the M−I domain walls.[25,26]

The effects of the two types of Peltier junctions on the motion of a single domain wall can be counteracting: the Cr−$W_xV_{1-x}O_2$ Peltier junction drives the I phase to expand on the low-V (electron source) end of the nanobeam, whereas the $W_xV_{1-x}O_2$ M−I Peltier junction drives the I phase to expand on the high-V (electron sink) end. In the optical interrogations of suspended nanobeams (see Supporting Information), the I phase appears mostly on the low-voltage end of the nanobeam, suggesting that the Cr−$W_xV_{1-x}O_2$ Peltier effect is dominant in determining the direction of domain wall propagation in suspended nanobeams.

The experimental data presented here show that the spontaneous M−I phase oscillations exhibited by current-biased $W_xV_{1-x}O_2$ nanobeams occur through the axial drift of a single M−I domain wall caused by Joule heating, the Peltier effect, the MIT, heat dissipation, and the charging/discharging of a shunt capacitor. They also demonstrate that one-dimensional nanostructures provide an ideal model system for studying the dynamics of confined domains and domain boundaries. Due to their nanoscale dimensions and controlled current path, the suspended nanobeams display a domain behavior that is well-defined and amenable for detailed study, illuminating the microscopic mechanism of domain motion.

Acknowledgment. We thank K. Maher for her scientific discussion. This work is supported by Samsung Electronics, NSF, and the Packard Foundation.

Supporting Information Available: Two videos obtained from devices incorporating single $W_{0.01}V_{0.99}O_2$ nanobeams: in video 1, the nanobeam is suspended, and in video 2, the nanobeam is lying on a substrate. This material is available free of charge via the Internet at http://pubs.acs.org.

References

(1) Christian, J. W. *The Theory of Transformations in Metals and Alloys*; Pergamon Press: Oxford, 1965.
(2) Chen, C.-C.; Herhold, A. B.; Johnson, C. S.; Alivisatos, A. P. *Science* **1997**, *276*, 398−401.
(3) Jacobs, K.; Zazisky, D.; Scher, E. C.; Herhold, A. B.; Alivisatos, A. P. *Science* **2001**, *293*, 1803−1806.
(4) Zaziski, D.; Prilliman, S.; Scher, E. C.; Casula, M.; Wickham, J.; Clark, S. M.; Alivisatos, A. P. *Nano Lett.* **2004**, *4*, 943−946.
(5) Brus, L. E.; Hackless, J. A. W.; Stillinger, F. H. *J. Am. Chem. Soc.* **1996**, *118*, 4834−4838.
(6) Spanier, J. E.; Kolpak, A. M.; Urban, J. J.; Grinberg, I.; Yun, W. S.; Ouyang, L.; Rappe, A. M.; Park, H. *Nano Lett.* **2006**, *6*, 735−739.
(7) Yun, W. S.; Urban, J. J.; Gu, Q.; Park, H. *Nano Lett.* **2002**, *2*, 447−450.
(8) Fisher, B. *J. Appl. Phys.* **1978**, *49*, 5339−5341.
(9) Tritt, T. M.; Subramanian, M. A. *MRS Bull.* **2006**, *31*, 188−193.
(10) Mott, N. F. *Metal-Insulator Transitions*, 1st ed.; Taylor & Francis: New York, 1974.
(11) Eyert, V. *Ann. Phys.* (*Weinheim, Ger.*) **2002**, *11*, 650−702.
(12) Biermann, S.; Poteryaev, A.; Lichtenstein, A. I.; Georges, A. *Phys. Rev. Lett.* **2005**, *94*, 026404.
(13) Rakotoniaina, J. C.; Mokranitamellin, R.; Gavarri, J. R.; Vacquier, G.; Casalot, A.; Calvarin, G. *J. Solid State Chem.* **1993**, *103*, 81−94.
(14) Jin, P.; Nakao, S.; Tanemura, S. *Thin Solid Films* **1998**, *324*, 151−158.
(15) Jin, P.; Tazawa, M.; Yoshimura, K.; Igarashi, K.; Tanemura, S.; Macak, K.; Helmersson, U. *Thin Solid Films* **2000**, *375*, 128−131.
(16) Chudnovskiy, F.; Luryi, S.; Spivak, B. In *Future Trends in Microelectronics*: *the Nano Millenium*; Luryi, S., Xu, J. M., Zaslavsky, A., Eds.; Wiley-Interscience: New York, 2002, pp 148−155.
(17) Kim, H. T.; Chae, B. G.; Youn, D. H.; Maeng, S. L.; Kim, G.; Kang, K. Y.; Lim, Y. S. *New J. Phys.* **2004**, *6*, 51−59.
(18) Greenberg, C. B. *Thin Solid Films* **1994**, *251*, 81−83.
(19) Guiton, B. S.; Gu, Q.; Prieto, A. L.; Gudiksen, M. S.; Park, H. *J. Am. Chem. Soc.* **2005**, *127*, 498−499.
(20) Wu, J.; Gu, Q.; Guiton, B. S.; de Leon, N.; Lian, O.; Park, H. *Nano Lett.* **2006**, ASAP.
(21) Sawano, F.; Terasaki, I.; Mori, H.; Mori, T.; Watanabe, M.; Ikeda, N.; Nogami, Y.; Noda, Y. *Nature* **2005**, *437*, 522−524.
(22) Bullock, D. C.; Epstein, D. J. *Appl. Phys. Lett.* **1970**, *17*, 199−201.
(23) Taketa, Y.; Kato, F.; Nitta, M.; Haradome, M. *Appl. Phys. Lett.* **1975**, *27*, 212−214.
(24) Taketa, Y.; Furugochi, R. *Appl. Phys. Lett.* **1977**, *31*, 405−406.
(25) Fisher, B. *J. Phys. C*: *Solid State Phys.* **1976**, *9*, 1201−1209.
(26) Fisher, B. *J. Phys. C*: *Solid State Phys.* **1975**, *8*, 2072.

NL0624768